nature chemistry

Article

https://doi.org/10.1038/s41557-023-01252-8

Site-specific bioorthogonal protein labelling by tetrazine ligation using endogenous β-amino acid dienophiles

Received: 3 May 2022

Accepted: 24 May 2023

Published online: 3 July 2023

Check for updates

Daniel Richter [1,2], Edgars Lakis [1,2] & Jörn Piel [1]

The tetrazine ligation is an inverse electron-demand Diels–Alder reaction widely used for bioorthogonal modifications due to its versatility, site specificity and fast reaction kinetics. A major limitation has been the incorporation of dienophiles in biomolecules and organisms, which relies on externally added reagents. Available methods require the incorporation of tetrazine-reactive groups by enzyme-mediated ligations or unnatural amino acid incorporation. Here we report a tetrazine ligation strategy, termed TyrEx (tyramine excision) cycloaddition, permitting autonomous dienophile generation in bacteria. It utilizes a unique aminopyruvate unit introduced by post-translational protein splicing at a short tag. Tetrazine conjugation occurs rapidly with a rate constant of 0.625 (15) M^{-1} s^{-1} and was applied to produce a radiolabel chelator-modified Her2-binding Affibody and intracellular, fluorescently labelled cell division protein FtsZ. We anticipate the labelling strategy to be useful for intracellular studies of proteins, as a stable conjugation method for protein therapeutics, as well as other applications.

Bioorthogonal chemistry has found widespread use in biological research and medicine by bringing rare chemical transformations into the diverse and crowded environment of living cells[1]. The rapid pace of innovation in the field has resulted in the development of numerous reactions that can be performed in biological settings. Site-specific chemical protein modifications have found many applications in biomedicine ranging from the incorporation of various biophysical probes[2] to protein–drug conjugates[3]. Despite their utility, a number of drawbacks still exist. First, the bioconjugation of natural amino acids is often complicated by the presence of additional reactive sites in a protein. For instance, cysteine side-chain thiols have been used extensively in nucleophilic addition reactions; however, competing reactions with disulfide moieties or free thiols diminish the regioselectivity. Second, non-proteinogenic amino acids offer functionalities outside of the naturally occurring chemical space but can be challenging to incorporate into proteins. For example, carbonyl- and alkyne-functionalized amino acids have been used for their bioorthogonal reactivity with nucleophiles and azides, respectively[4–6]. Third, conjugation reactions are suitable for biological applications only if they are spontaneous, selective, fast and possible at low reagent concentrations, and many reactions developed in vitro are not suitable for in vivo applications[7].

One of the most useful in vivo bioorthogonal transformations is the ligation of tetrazines with reactive strained dienophiles through an inverse electron-demand Diels–Alder (IEDDA) cycloaddition[8,9]. This rapid reaction is more selective than alternative bioorthogonal reactions, such as the Staudinger ligation[10], copper-catalysed azide-alkyne cycloaddition[11], strain-promoted azide-alkyne cycloaddition[12] or variants of the Pictet–Spengler reaction[13]. A limitation of the tetrazine technology, however, is the incorporation of non-natural dienophiles into protein targets[14]. This is typically achieved by genetic code expansion[15] or through enzyme-mediated ligation[16–20], which require the addition of an external dienophile-carrying reagent. The de novo cellular production of a unique dienophile directly on the target protein would eliminate the need for external reagents, lessen the synthetic effort,

[1]Institute of Microbiology, Eidgenössische Technische Hochschule (ETH) Zürich, Zürich, Switzerland. [2]These authors contributed equally: Daniel Richter, Edgars Lakis. e-mail: jpiel@ethz.ch

https://doi.org/10.1038/s41557-023-01252-8

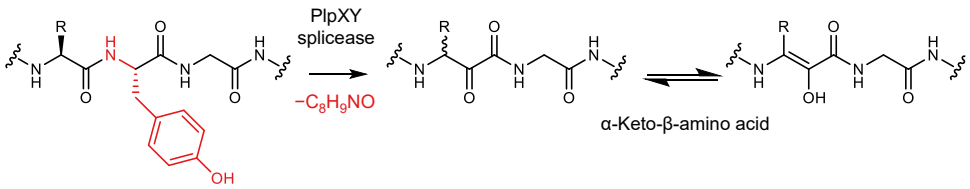

Fig. 1 | Net reaction of tyramine splicing. In the post-translational modification, the PlpXY splicease excises a tyramine equivalent (red, C_8H_9NO) at the tyrosine-glycine (YG) motif. R: amino acid side chain. The product is configurationally unstable at the former α-carbon due to enolization.

and limit side reactivity and toxicity arising from substrate molecules and codon ambiguity.

In this article, we leveraged a naturally occurring transformation in ribosomally synthesized and post-translationally modified peptide (RiPP) biosynthesis to accomplish facile in vivo installation of IEDDA sites. RiPPs are biosynthesized by post-translational maturation enzymes that act on ribosomally produced precursor peptides and install a wide range of non-canonical amino acids with diverse functionalities[21,22]. After maturation, a modified peptide is usually proteolytically cleaved and exported from the cell. We recently discovered an unusual bacterial RiPP modification that converts amino acids X within precursor XYG motifs to the corresponding α-keto-β-amino acid residue, in the following referred to as ketoamide (Fig. 1)[23].

This remarkable modification is achieved by the splicease complex PlpXY, of which PlpX belongs to the radical *S*-adenosylmethionine (rSAM) superfamily. It catalyses a formal net excision of a tyramine moiety from tyrosine and reconnection of the spliced peptide ends, thus fusing the remaining amide carbonyl of tyrosine to the carbonyl function of the preceding amino acid. The resulting homologized X residue, an α-keto-β-amino acid derivative, is predicted to possess unique chemical reactivity in the cellular proteome. Here we leveraged this peptide modification to achieve in vivo bioorthogonal IEDDA labelling of target proteins in a bacterial cell requiring only the external addition of a probe. While the previously discovered natural ketoamides carry side chains derived from non-glycine units, here we used an engineered GYG site to minimize steric hindrance during cycloaddition and enable a final aromatization step. We produced proteins containing the glycine-derived aminopyruvate residue in bacteria and site-selectively conjugated tetrazine probes using IEDDA cycloaddition. The utility of the technology was demonstrated by conjugating a Her2/ErbB2-binding Affibody with a dodecane tetraacetate chelator for use in cancer target radiolabelling and by fluorescently labelling the bacterial cell division protein FtsZ in fixed *Escherichia coli* cells.

Results and discussion

Reaction of aminopyruvate with tetrazines

Inspired by reports of tetrazine IEDDA cycloaddition to synthetic aldehydes[24] and ketones[25], we tested whether ketoamides also possess similar reactivity. We hypothesized that either the ketoamide enol form or an enamine spontaneously generated in the presence of biological amines could serve as the dienophile for IEDDA cycloaddition. Nevertheless, we did not find literature precedents where ketoamide functional moieties act as a dienophile.

For model reactions we synthesized the aminopyruvate derivative **1** to study its IEDDA reactivity and the catalytic effect of L-proline and divalent metal ion additives. Synthetic compound **1** was incubated with 3,6-di-2-pyridyl-1,2,4,5-tetrazine (**2**) for 18 h in aqueous solution at 37 °C (Fig. 2a). To individual test reactions we added L-proline, Ca^{2+} or Mg^{2+}. Product formation and the effect of additives on product yield was monitored by liquid chromatography–mass spectrometry (LC–MS) comparing apparent relative conversions by MS intensities (Fig. 2d,e). Model aminopyruvate IEDDA reactivity data showed pyridazine formation regardless of additives in aqueous conditions. Neither L-proline nor other additives resulted in substantially higher conversion in water. A 20-fold increase in yield, however, was observed in phosphate-buffered saline (PBS), a buffer that emulates in vivo conditions (Fig. 2d,e). The reported proline-catalysed IEDDA to synthetic aldehydes and ketones proceeds through the corresponding enamine intermediates; however, an enolization is probably sufficient for the aminopyruvate cycloaddition and might benefit from the presence of phosphate, which can act as enolization catalyst[26]. We observed accelerated enolization of **1** in PBS ($k_{obs} = 1.05 \times 10^{-4}$) compared with water ($k_{obs} = 2.5 \times 10^{-7}$) by deuterium exchange and LC–MS (Supplementary Fig. 22). Additionally, we observed an increased amount of enol present in PBS compared with D_2O (Fig. 2c, 28.2% (2.4%) in D_2O compared with 41.9% (1.9%) in PBS, $P = 0.0016$). The stability of conjugates **4** and **5** was analysed by LC (Fig. 2f,g) over 3 days, which showed less than 25% decrease in UV signal after 72 h.

Reaction kinetics were analysed in PBS by ultraviolet (UV)–visible spectrometry. The decrease of the absorption maximum at 515 nm for tetrazine **2** at 25 °C was recorded over 30 min (Fig. 2b). The acquired data follow a second-order reaction mechanism affording a second-order rate constant of 0.625 (15) $M^{-1} s^{-1}$. For lower concentrations of tetrazine in solution we observed a systematic deviation from the rate law in the first 5 min of reaction progress (Supplementary Fig. 20e). This accelerated rate might indicate excess enol that is more rapidly consumed than the formation of enol. However, we were not able to test the reaction behaviour more carefully during the initial seconds to fully characterize this behaviour. We additionally tested the less electronically activated (4-(1,2,4,5-tetrazin-3-yl)phenyl)methanamine **8**, which showed a slower second-order rate constant of $k_{obs} = 0.049$ (9) $M^{-1} s^{-1}$, although for this example we observed a faster rate constant in H_2O of $k_{obs} = 0.18$ (5) $M^{-1} s^{-1}$ (Supplementary Fig. 21). While these kinetic values are slower than conventional strained dienophiles, the reasonably fast kinetics of the model reaction encouraged us to test next whether it is possible to enzymatically incorporate the glycine-derived aminopyruvate moiety into proteins.

Reactive site incorporation and in vitro conjugation

As mentioned, ketoamide units are biologically generated by the post-translational machinery of spliceotides, a family of bacterial ribosomal peptides that we had discovered previously. For this study we tested the prototype splicease PlpXY from the cyanobacterium *Pleurocapsa* sp. PCC 7319, which naturally acts on MYG and LYG peptide sites to generate the corresponding ketoamides with methionine and leucine side chains. Studies on precursor analogues showed that a point mutant of the natural substrate PlpA3 with an engineered GYG motif is also accepted as a substrate and converted to the aminopyruvate-containing product lacking a ketoamide side chain[23]. The mutation to the sterically less demanding residue was hoped to facilitate tetrazine cycloadditions in complex cellular environments. To test whether IEDDA is compatible with a large peptide, an N-terminally His_6-tagged variant of the GYG precursor mutant, His_6-PlpA3-M5G (117 amino acids), was co-produced with the splicease PlpXY in *E. coli* by expression from the plasmids *plpA3-M5G*/pACYCDuet-1 and *plpXY*/pRSFDuet (Supplementary Table 2). Isolation of His_6-PlpA3-M5G by Ni-nitrilotriacetic

https://doi.org/10.1038/s41557-023-01252-8

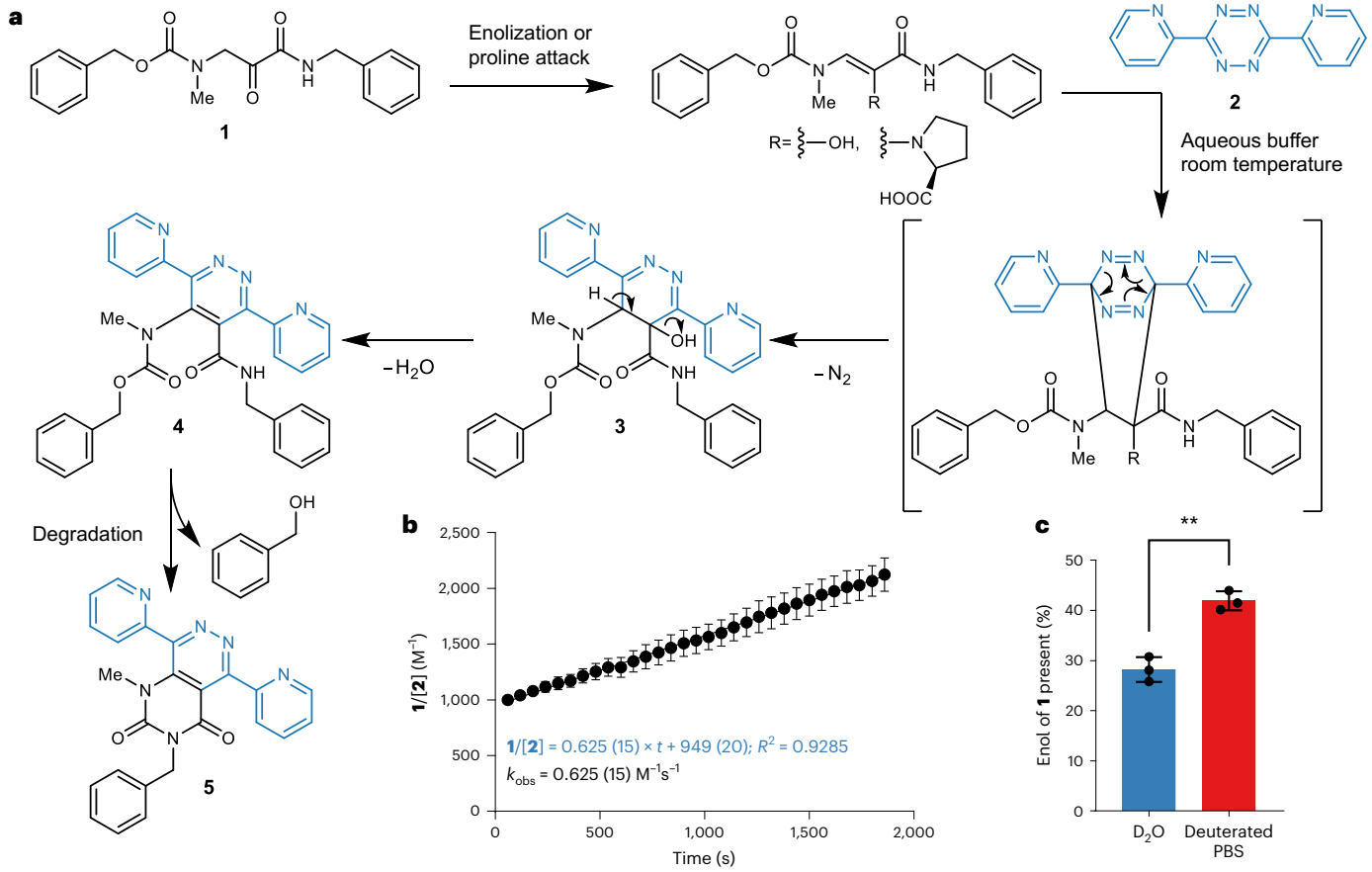

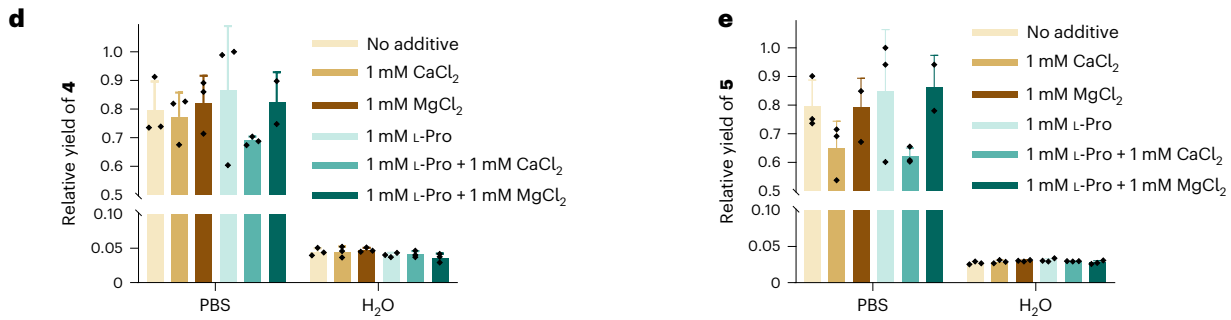

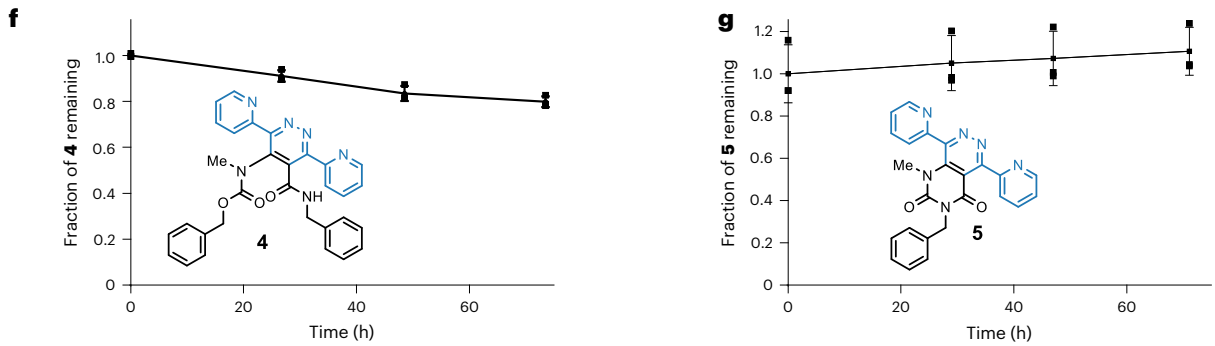

Fig. 2 | Test reactions of the aminopyruvate model compound 1 to explore the feasibility of pyridazine formation in vitro. a, Proposed reaction between **1** and 3,6-di-2-pyridyl-1,2,4,5-tetrazine **2** to yield intermediate **3**, and pyridazine products **4** and **5**. **b**, Reaction kinetics in PBS pH 7.4 measured by visible light spectrometry. The decrease in absorbance at 515 nm of tetrazine **2** was measured over time and fitted to a second-order reaction kinetic equation yielding an apparent rate constant of k_{obs} = 0.625 (15) $M^{-1} s^{-1}$ in 30% DMSO in H_2O (n = 3 independent experiments). Points describe mean; error bars describe standard deviation. **c**, Enol form of **1** present in solution in D_2O or deuterated PBS (28.2% (2.4%) in D_2O, 41.9% (1.9%) in PBS, P = 0.0016 by a two-tailed t-test) measured by deuterium exchange and MS (n = 3 independent experiments). Bars describe mean; error bars describe standard deviation. **d**,**e**, Effect of medium, L-proline and divalent metal ion additives on the yields of pyridazine **4** (**d**) and **5** (**e**), estimated by MS product ion abundance and relative product formation (n = 3 independent experiments). Bars describe mean; error bars describe standard deviation. **f**,**g**, Stability of conjugate **4** (**f**) and **5** (**g**) over time in 50% acetonitrile in H_2O, assessed by UV signal (280 nm). The line connects mean values; error bars represent standard deviations (n = 3 independent experiments).

https://doi.org/10.1038/s41557-023-01252-8

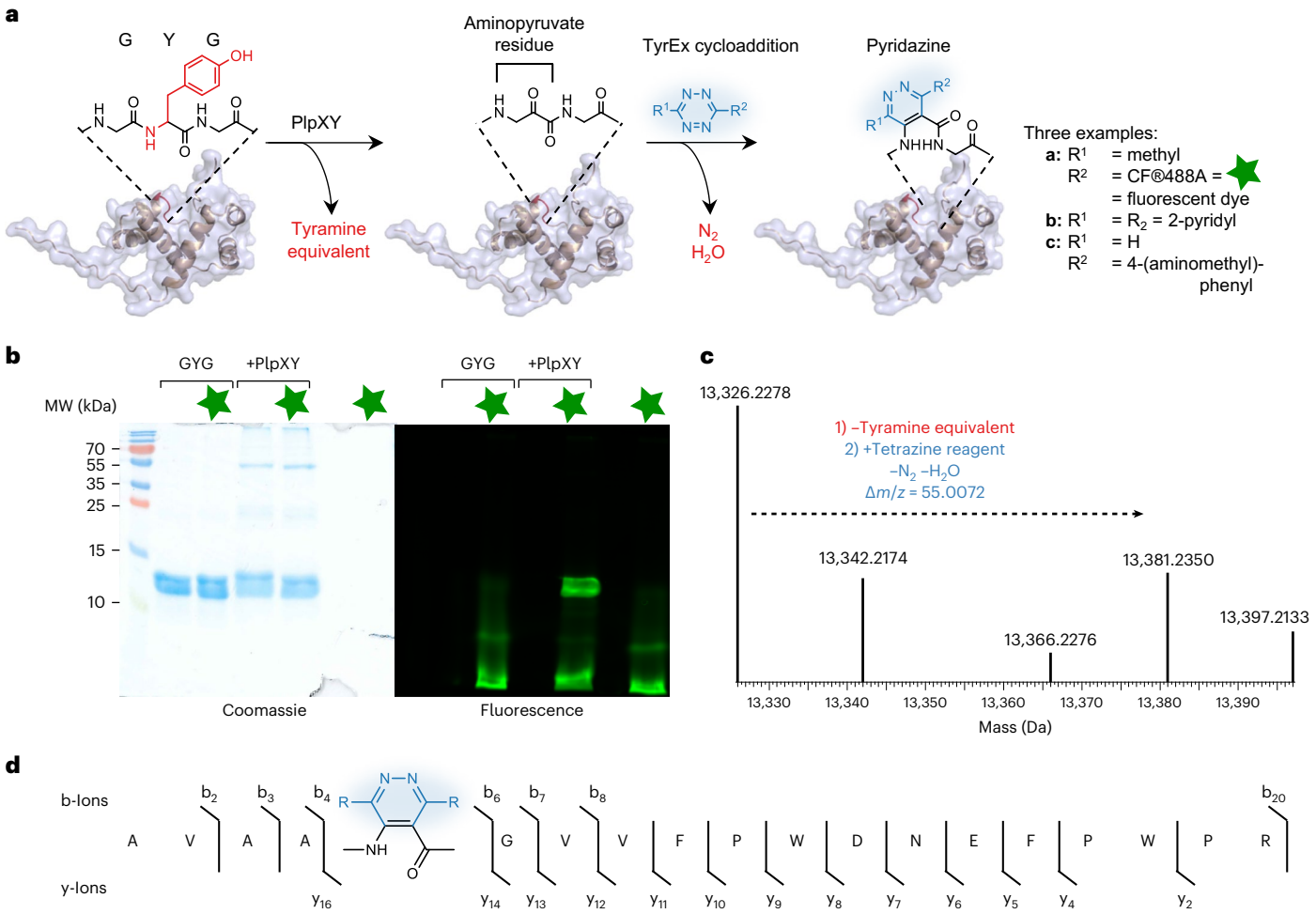

Fig. 3 | In vitro peptide conjugation of His_6-PlpA3-M5G with tetrazines. a, Overall tyramine excision (TyrEx) strategy for labelling of His_6-PlpA3-M5G: PlpXY expressed in the cell installs aminopyruvate site-specifically in the target biomolecule at a GYG-containing motif. Splicing results in a mass loss of −135.0757 Da ($-C_8H_9NO$). The post-translationally modified product reacts tetrazine derivatives to form the pyridazyl protein conjugates **a**–**c**. Structures are based on models calculated with AlphaFold[47,48]. **b**, Conjugation of His_6-PlpA3-M5G with a fluorescent tetrazine probe analysed by SDS–PAGE. GYG: unmodified His_6-PlpA3-M5G molecular weight (MW) 13.3 kDa. +PlpXY: His_6-PlpA3-M5G was co-produced with PlpXY to yield the aminopyruvate-containing product (MW 13.2 kDa). The CF®488A fluorophore (**6**) was imaged by gel fluorescence using a 488 nm excitation and 532/528 nm emission filter. The experiment was performed once. **c**, Deconvoluted electrospray ionization–mass spectra (ESI–MS) showing ions for the substrate (His_6-PlpA3-M5G, *m/z* calculated 13,326.2112, found 13,326.2278) and the cycloaddition product using tetrazine **2** (*m/z* calculated 13,381.2071, found 13,381.2350). **d**, Observed y- and b-ions for the ESI–MS/MS fragmentation of a trypsinized reaction product localizing the cycloaddition site (blue).

acid (NTA) affinity purification and subsequent in vitro conjugation with tetrazines verified successful conversion of the substrate to the aminopyruvate-containing product by PlpXY (Fig. 3 and Supplementary Figs. 24 and 25). Using the affinity-purified protein, we next investigated IEDDA reactions of spliced His_6-PlpA3-M5G with a range of tetrazine reagents (Fig. 3a). Tetrazine **2** was added to the isolated protein in a phosphate-based buffer (50 mM NaH_2PO_4, 300 mM NaCl and 250 mM imidazole, pH 8.0) and incubated at 20 °C for 18 h, similar to experiments with the model compound in PBS. Protein conjugation with the tetrazine probe **2** was confirmed by MS analysis and subsequent mass deconvolution (product *m/z* calculated 13,381.2071; observed 13,381.2350 in Fig. 3c). Limited conversion is due to the incomplete enzymatic step during co-expression of substrate and PlpXY (Supplementary Fig. 24). Notably, in tandem mass spectrometry (MS/MS) analyses, b- and y-ions of the labelled peptide displayed a mass change of +55.0099 relative to the His_6-PlpA3-M5G precursor, indicative of the incorporation of the tetrazine probe at the expected aminopyruvate site (Fig. 3d). A commercially available fluorescent tetrazine derivative, CF®488A (**6**), was also tested in IEDDA reactions with the aminopyruvate-containing His_6-PlpA3-M5G, and similar results were obtained (Supplementary Fig. 31 and 32). Fluorophore incorporation was verified by gel electrophoresis followed by fluorescence imaging (Fig. 3b). By splicing the target protein to generate bioconjugation substrates in vivo and subsequent in vitro IEDDA cyclization, we were able to generate labelled His_6-PlpA3-M5G after 18 h at mild conditions. We termed this method TyrEx (tyramine excision) cycloaddition.

In vitro production of Her2-binding affibody conjugates

After establishing the TyrEx cycloaddition in the context of the natural splicease substrate, we asked whether it can be implemented for non-native target proteins unrelated to spliceotides or RiPPs. We previously established that ketoamide production does not require the RiPP leader. This permits the incorporation of ketoamide moieties into diverse proteins at C-, N-terminal and internal positions in *E. coli* by integrating a ten-residue splice tag[27]. Here we considered antigen-binding conjugates, which are widely used in targeted drug delivery[28], positron emission tomography[29] and near-infrared[30] in vivo imaging, and for antigen inactivation by binding[31]. This therapeutic and diagnostic class

https://doi.org/10.1038/s41557-023-01252-8

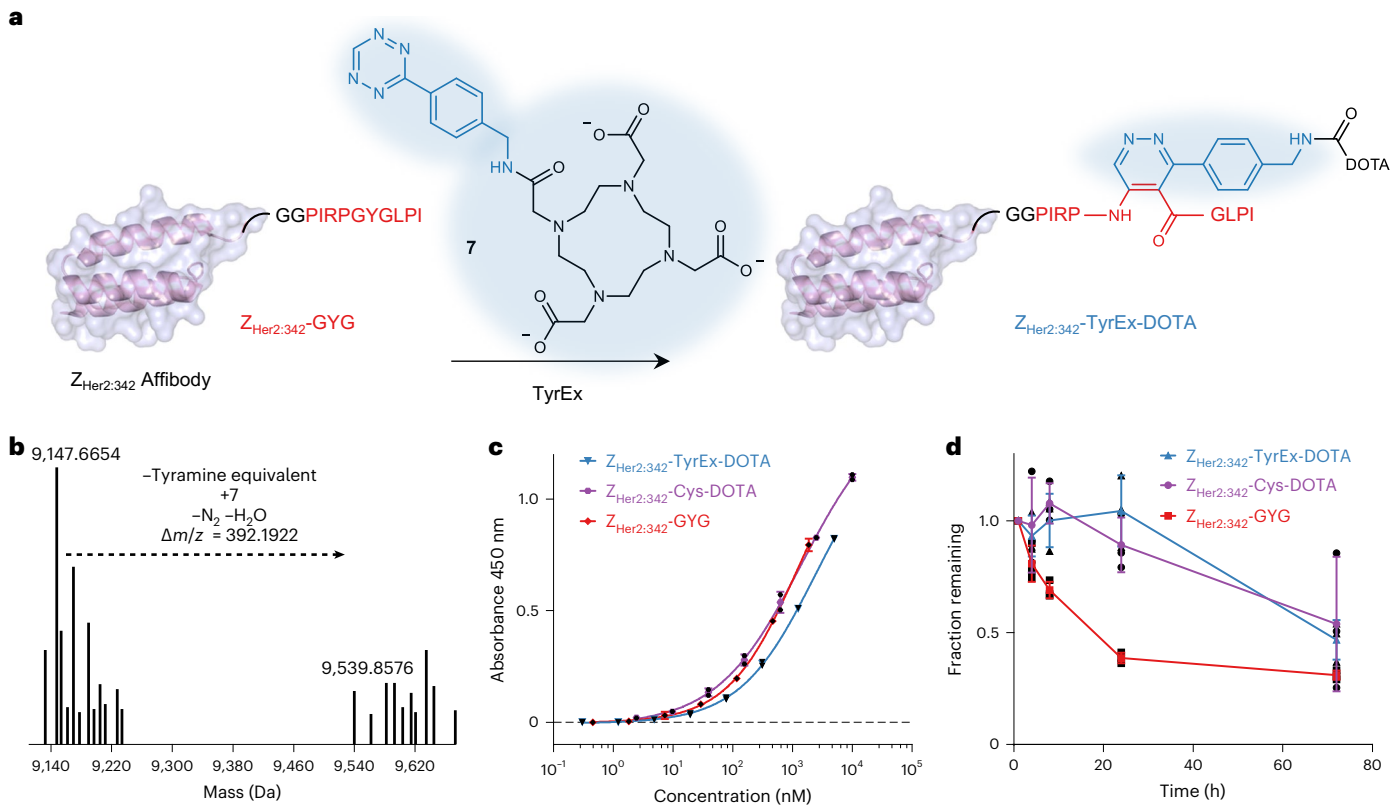

Fig. 4 | Production of a Her2-binding Affibody conjugate for radiolabelling by TyrEx cycloaddition. a, Scheme for generating the $Z_{Her2:342}$-DOTA conjugate. Cartoon visualization of the $Z_{Her2:342}$ Affibody based on crystal structures (PDB accession 3MZW)[49] with the C-terminal splicease tag (in red, GG serves as a linker). In vivo splicing and subsequent in vitro conjugation to DOTA-tetrazine (**7**) yields conjugates for radiolabelling. **b**, Deconvoluted MS spectrum of $Z_{Her2:342}$-GYG (m/z calculated 9,147.6540, found 9,147.6654) and the DOTA conjugate ($Z_{Her2:342}$-TyrEx-DOTA, m/z calculated 9,539.8277, found 9,539.8576). **c**, ELISA to detect Affibody binding to the recombinant Her2 extracellular domain immobilized on a 96-well plate. There was no significant difference between $Z_{Her2:342}$-TyrEx-DOTA and $Z_{Her2:342}$-Cys-DOTA ($n = 2$ independent experiments, $P = 0.3131$ by a two-tailed t-test with Welch's correction). **d**, Stability of the $Z_{Her2:342}$-TyrEx-DOTA conjugate, its precursor protein, and $Z_{Her2:342}$-Cys-DOTA in human blood plasma over 72 h at 37 °C, measured by LC–MS. The line connects mean values; error bars represent standard deviations ($n = 3$ independent experiments).

of molecules can be divided into antibody-based (for example, antibody–drug conjugates, light and heavy chain fragments[32], and nanobodies)[33] and engineered non-antibody protein-binding scaffolds (for example, DARPins[34] and Affibodies)[35]. While the first category is produced mainly in eukaryotic cells, the second can be readily produced and genetically manipulated in *E. coli*. We therefore selected a Her2/ErbB2-binding Affibody ($Z_{Her2:342}$) as a model protein[36]. The α-helical Affibody (8.3 kDa) is highly water soluble and substantially smaller than antibody fragments (4×) or antibodies (20×). For diagnostic radiolabelling purposes, Affibodies are conjugated to ligands that bind radioactive metals, enabling tumour imaging in vivo. Usually, these conjugates are prepared through cysteine-maleimide addition with derivatives of 1,4,7,10-tetraazacyclododecane-1,4,7,10-tetraacetate (DOTA), utilizing a cysteine residue at the Affibody C-terminus[37]. Maleimide conjugations have been reported to suffer from hydrolytic cleavage and thiol exchange reactions in vivo[38,39]. We therefore envisioned that linking the Affibody by TyrEx addition would alleviate these shortcomings and require fewer preparatory steps than the thiol chemistry as no reduction step is needed and the reaction selectively proceeds in the presence of other biomolecules.

To prepare the dienophile substrate, we generated an N-terminally His_6-tagged Affibody His_6-$Z_{Her2:342}$ hybrid with a C-terminally fused 10-amino-acid minimal PlpA2 core containing an engineered GYG motif (splice tag sequence in Fig. 4a). The protein, designated His_6-$Z_{Her2:342}$-GYG, was heterologous co-produced in *E. coli* together with the splicease PlpXY by expression from pACYC and pRSF vectors (Supplementary Table 2). Affinity purification and LC–MS/MS analysis suggested the presence of the reactive aminopyruvate residue (Supplementary Figs. 33 and 34). We performed the IEDDA reaction on spliced $Z_{Her2:342}$-GYG with the DOTA tetrazine **7** (Fig. 4a). Affinity-purified aminopyruvate-containing His_6-$Z_{Her2:342}$-GYG was added with **7** in PBS buffer. Incubation at 37 °C for 18 h yielded the Affibody-DOTA conjugate ($Z_{Her2:342}$-TyrEx-DOTA), which was confirmed by LC–MS analysis and subsequent mass deconvolution (product m/z calculated 9,539.8277; observed 9,539.8553 in Fig. 4b). MS/MS analysis confirmed localization of the modification to the expected site (Supplementary Figs. 35 and 36).

$Z_{Her2:342}$-TyrEx-DOTA and the precursor protein $Z_{Her2:342}$-GYG were purified by reversed-phase high-performance liquid chromatography (HPLC) and analysed by an enzyme-linked immunosorbent assay (ELISA) with Her2 immobilized on 96-well plates to assess whether binding functionality is preserved (Fig. 4c). For comparison, $Z_{Her2:342}$ with a C-terminal cysteine was expressed from a pACYC vector in *E. coli* and conjugated with maleimide-DOTA as previously described to obtain $Z_{Her2:342}$-Cys-DOTA[37]. The ELISA suggested comparable binding ($P = 0.3131$) affinities for $Z_{Her2:342}$-TyrEx-DOTA ($K_{D,app}$ = 2,348 nM) and $Z_{Her2:342}$-Cys-DOTA ($K_{D,app}$ = 1,432 nM).

To characterize the stability of the two conjugates, $Z_{Her2:342}$-TyrEx-DOTA and $Z_{Her2:342}$-Cys-DOTA as well as the precursor fusion protein $Z_{Her2:342}$-GYG were incubated in human blood plasma for up to 3 days at 37 °C (Fig. 4d). While there was no significant difference between the two conjugates, the precursor tagged with the

Table 1 | Tested splice tag sequences and locations in FtsZ

Insertion site	Tag peptide sequence	Modified
N-terminus	GGPIRPGYGLPI	–
	GAVAAGYGVVFPG	–
E35	GGPIRPGYGLPI	–
A53	GGPIRPLYGLPI	–
	GGPIRPGYGLPI	–
G55-Q56	GPIRPLYGLPI	–
	GPIRPGYGLPI	–
	GPIRPGYGLPILEGSTI	–
	IGSTLEGGPIRPGYGLPI	–
	IGSTLEGGPIRPGYGLPILEGSTI	+
S218	GGPIRPGYGLPI	–
L325-D337	FPIRPGYGLPI	–
	AVAGYGLPI	–
E350-Q364	PLFPIRPGYGLPI	+
C-terminus	GGPIRPGYGLPI	–
	GGAVAAGYGVVFP	–

'–' denotes FtsZ variants that were not accepted; '+' denotes accepted substrates.

GGPIRPGYGLPI sequence was degraded very quickly with below 50% remaining after 24 h. MS analysis of the degradation products suggested that the proline-glycine bond N-terminal to the modification site is degraded (Supplementary Fig. 38). MS data for the TyrEx conjugate suggested the same degradation site (Supplementary Fig. 38). Therefore, we hypothesize that the detected degradation is not a consequence of the conjugation but of the peptide sequence itself, as the conjugated protein degraded more slowly than the unconjugated precursor (Fig. 4d). We hope to leverage any of the 27 other characterized or 939 predicted splicease systems reported by our group for future applications to avoid the issue of degradation[40].

Confocal imaging of labelled FtsZ in *E. coli* cells

With protein bioconjugation established in vitro, further experiments aimed to establish intracellular labelling. As the cellular target, we selected the cell division protein FtsZ for fluorescence imaging. FtsZ is a polymeric cytoskeletal protein that during cell division localizes at the nascent septum of prokaryotic cells and thus guides cell wall formation[41,42]. Due to its focused localization, fluorescent variants can be distinguished readily from non-specific labelling, and the catalytic activity and inter-monomer interactions required for functional FtsZ were useful features to assess potential functional disturbances caused by the TyrEx modification that impair cell division. We probed the surface of *E. coli* FtsZ by inserting splice tag sequences at eight locations across the protein (Table 1 and Fig. 5a). Different splicease recognition motifs containing the GYG region were genetically introduced into His_6-tagged FtsZ at either the N- or the C-terminus, or inserted at internal sites between amino acids G55-Q56, A53-V54, E35-G36 or S218-E219 that have been reported before as suitable for small peptide insertions[41,43]. In addition, 11- and 13-amino acid segments L325-D337 and E350-Q364, respectively, in the intrinsically disordered FtsZ 'spring' region were substituted with the splicease motif sequence.

First, we tested production of aminopyruvate-modified FtsZ variants for the constructs by heterologous co-production with the PlpXY splicease in *E. coli*. His_6-tagged target proteins were expressed from pACYCDuet-1 and pRM006 plasmids (the latter purchased from Addgene, #98922) and purified by Ni^{2+}-affinity chromatography for LC–MS analysis. While most of the tested constructs yielded soluble FtsZ variants, only the two variants FtsZ-E350-Q364 and FtsZ-G55-Q56 were successfully spliced at the GYG site, as verified by LC–MS/MS analysis (Supplementary Figs. 39–42).

Subsequently, we conducted a test conjugation in vitro with the aminopyruvate-containing FtsZ variant G55-Q56 using a fluorescent CF488A® tetrazine probe (**6**) and assessed labelling by gel electrophoresis imaging (Fig. 5b). For the assays, the His_6-FtsZ-G55-Q56 protein solution prepared by Ni^{2+}-affinity chromatography was mixed with **6** (1 μM) and incubated for 18 h at 37 °C. The reaction mixtures were directly loaded on the polyacrylamide gel. Gel fluorescence imaging and Coomassie staining showed a distinct band at the expected molecular weight region for FtsZ, while no fluorescence was observed in a control experiment using non-spliced protein.

With suitable FtsZ variants in hand, we next interrogated intracellular protein splicing, labelling, and imaging in the same cells. An *E. coli* strain was prepared carrying the two expression plasmids *ftsZ-G55*/pACYCDuet-1 and *plpXY*/pRSFDuet for the target protein FtsZ-G55-Q56 and the PlpXY splicease, respectively. 20 h after induction of expression in TB medium, *E. coli* cells were fixed with formaldehyde and permeabilized with Triton X-100. Bacteria were resuspended, mixed with **6** (10 μM) and shaken for 1 h at 37 °C. Subsequently, the cells were washed and analysed for cell phenotype by confocal laser scanning microscopy. These analyses revealed selective staining only for assays containing the FtsZ variant, the splicease, and the dye (Fig. 5c). Fluorescence is localized in the septum in the Z-ring structure as well as on poles of dividing cells where FtsZ is sequestered in granules that form at the cell poles in stationary phase[42,44]. Fluorescence of the cytoskeletal structure was not observed in cells producing FtsZ G55-Q55 alone (Fig. 5c, middle micrograph). In a time course experiment, we observed that co-expression of FtsZ with PlpXY was needed to proceed for at least 12 h for sufficient enzyme activity (Fig. 5d). These results showed that the TyrEx bioconjugation can fluorescently label proteins in cells by introducing a short peptide tag, thus providing an attractive alternative to existing intracellular labelling methods.

Conclusion

This study describes an additional tetrazine ligation strategy, termed TyrEx cycloaddition that is based on autonomous dienophile generation in a bacterial cell. The method utilizes a unique aminopyruvate unit incorporated into target proteins by enzymatic backbone splicing at a genetically introduced GYG site. IEDDA reactions between aminopyruvate residues and tetrazines probably proceed through the aminopyruvate enol form with a rate of ~0.625 M^{-1} s^{-1} in PBS buffer for the analysed model compound, slower than conventional strained dienophiles. The conjugate was shown to be stable over 72 h with no major degradation in vitro. The TyrEx cycloaddition was applied to site-specifically label the therapeutically relevant Her2/ErbB2 Affibody protein with the DOTA chelator for use in cancer target radiolabelling. In addition, the method allowed us to fluorescently label the cell division protein FtsZ in fixed *E. coli* cells via an inserted 24-residue sequence.

Several features of the TyrEx cycloaddition system make it attractive for protein conjugation. First, the protein splicing system is naturally not present in *E. coli* or mammalian cells, which makes the post-translational modification of target proteins bioorthogonal and genetically tractable. Second, the de novo cellular production of the dienophile directly on the target protein eliminates the need for incorporation of dienophiles by enzyme-mediated ligations or unnatural amino acid incorporation, often accompanied by low yields and interferences from codon reassignments. Third, the dienophile is located on the protein backbone, reducing the linker length to the label and effective size of the protein modification, making this method attractive for exact molecular distance measurements by Förster resonance energy transfer[45] or electron paramagnetic resonance[46]. TyrEx

https://doi.org/10.1038/s41557-023-01252-8

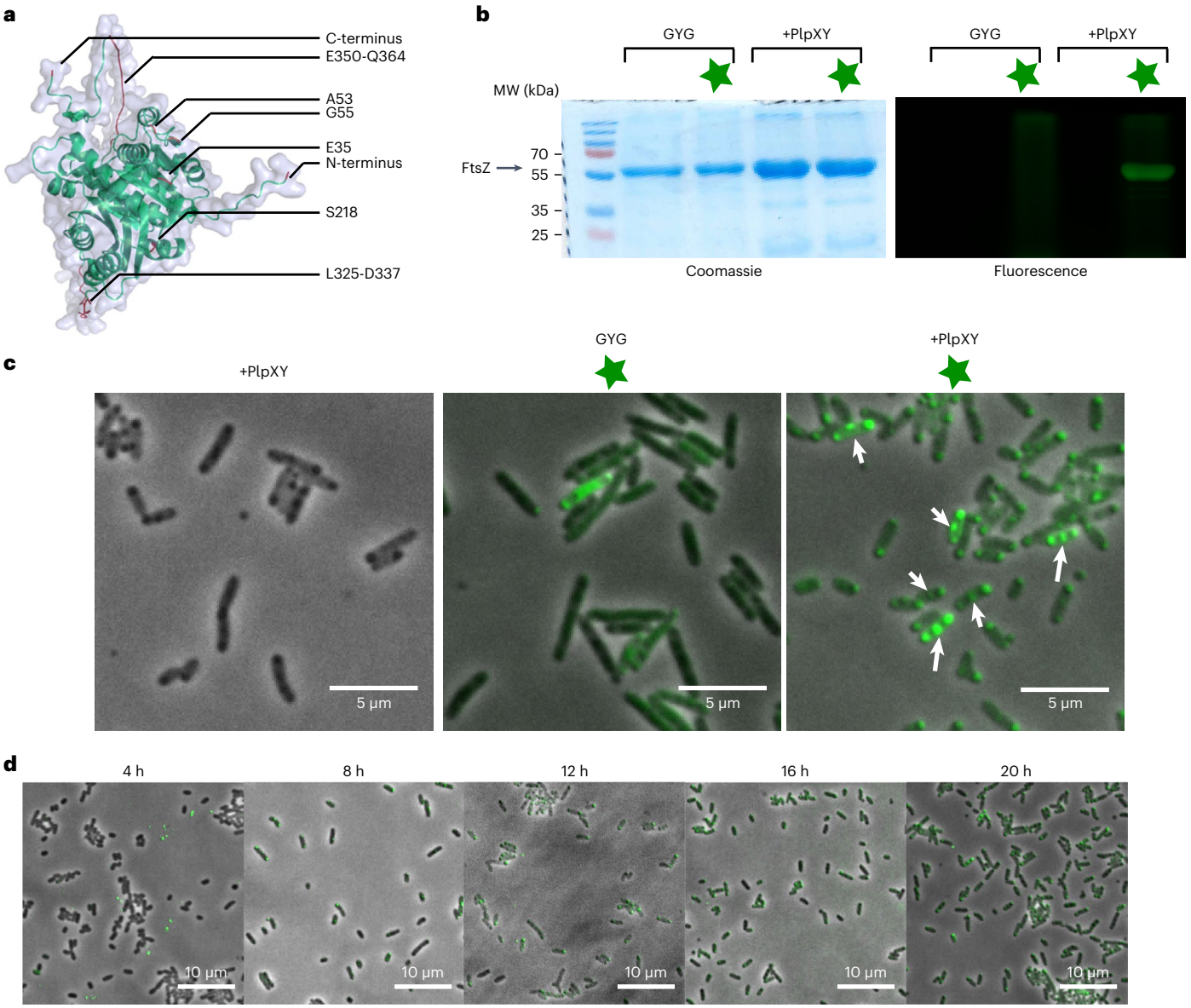

Fig. 5 | Imaging of FtsZ fluorescently labelled in vivo by TyrEx cycloaddition. **a**, Structure of FtsZ predicted with AlphaFold[47,48]. Studied tag locations are highlighted in red and labelled with black lines (see also Table 1). **b**, SDS–PAGE analysis of CF®488A (**6**) labelled FtsZ G55-Q56. The left gel shows Coomassie-stained protein bands; the right gel shows gel fluorescence using 488 nm excitation and 532/28 nm emission filter. Samples labelled +PlpXY were co-expressed with the splicease PlpXY. The star symbol denotes the addition of **6** (10 µM). The experiment was performed once. **c**, In situ fluorescence micrographs of fixed *E. coli* cells harbouring fluorescent FtsZ-G55-Q56. Fluorescent signals in the septum of cells are highlighted with white arrows. **d**, Fluorescence micrographs of cells cultured to the indicated time points after induction of protein expression. Overlaid images of brightfield illumination and 488 nm are shown. All representative microscopy images where manually selected from 3–12 images acquired for each condition.

conjugates can easily be prepared in few steps, lessen the synthetic effort, and limit side reactivity and toxicity arising from substrate molecules. Antigen-binding protein conjugates prepared through TyrEx thus provide an alternative strategy to existing methods that can alleviate shortcomings from other methods. Conjugates are functional and similarly stable in human blood plasma as other methods. In fluorescent protein labelling, the small size of the TyrEx tag (minimally ten amino acids) permits applications that are not compatible with the larger GFP-derived labels. However, the slower reaction kinetics can be limiting in some cases where the use of strained dienophiles will be more appropriate.

Regarding further optimization potential, FtsZ tested here required relatively elaborate tag optimization regarding length and location to achieve modification by PlpXY. In contrast, splicing has been more straightforward for five different other proteins in vitro using terminal as well as internal positions[27]. More processive spliceases (either natural homologues or engineered variants) and alternative and further shortened peptide tag sequences will further broaden the applicative use, as would an implementation of the method in eukaryotic cells. Efforts to develop such enhanced splicing systems are ongoing in our laboratory[40].

In vivo production of dienophiles for ligation with tetrazines expands the scope of bioorthogonal reactions for chemical biology, and simultaneously highlights the utility of the vast enzyme diversity from natural product biosynthesis outside their native context. We anticipate the labelling strategy to be useful for in vivo studies of cellular proteins, as a stable conjugation method for therapeutic and diagnostic proteins, and many other applications.

Online content

Any methods, additional references, Nature Portfolio reporting summaries, source data, extended data, supplementary information, acknowledgements, peer review information; details of author contributions and competing interests; and statements of data and code availability are available at https://doi.org/10.1038/s41557-023-01252-8.

References

1. Devaraj, N. K. The future of bioorthogonal chemistry. *ACS Cent. Sci.* **4**, 952–959 (2018).
2. Toseland, C. P. Fluorescent labeling and modification of proteins. *J. Chem. Biol.* **6**, 85–95 (2013).
3. He, R., Finan, B., Mayer, J. P. & DiMarchi, R. D. Peptide conjugates with small molecules designed to enhance efficacy and safety. *Molecules* **24**, 1855 (2019).
4. Sletten, E. M. & Bertozzi, C. R. Bioorthogonal chemistry: fishing for selectivity in a sea of functionality. *Angew. Chem. Int. Ed.* **48**, 6974–6998 (2009).
5. Reichert, A. J., Poxleitner, G., Dauner, M. & Skerra, A. Optimisation of a system for the co-translational incorporation of a keto amino acid and its application to a tumour-specific anticalin. *Protein Eng. Des. Sel.* **28**, 553–565 (2015).
6. Agarwal, P. et al. Hydrazino-Pictet-Spengler ligation as a biocompatible method for the generation of stable protein conjugates. *Bioconjugate Chem.* **24**, 846–851 (2013).
7. Nguyen, S. S. & Prescher, J. A. Developing bioorthogonal probes to span a spectrum of reactivities. *Nat. Rev. Chem.* **4**, 476–489 (2020).
8. Blackman, M. L., Royzen, M. & Fox, J. M. Tetrazine ligation: fast bioconjugation based on inverse-electron-demand Diels–Alder reactivity. *J. Am. Chem. Soc.* **130**, 13518–13519 (2008).
9. Oliveira, B. L., Guo, Z. & Bernardes, G. J. L. Inverse electron demand Diels–Alder reactions in chemical biology. *Chem. Soc. Rev.* **46**, 4895–4950 (2017).
10. Saxon, E., Armstrong, J. I. & Bertozzi, C. R. A "traceless" Staudinger ligation for the chemoselective synthesis of amide bonds. *Org. Lett.* **2**, 2141–2143 (2000).
11. Rostovtsev, V. V., Green, L. G., Fokin, V. V. & Sharpless, K. B. A stepwise Huisgen cycloaddition process: copper(I)-catalyzed regioselective "ligation" of azides and terminal alkynes. *Angew. Chem. Int. Ed.* **41**, 2596–2599 (2002).
12. Agard, N. J., Prescher, J. A. & Bertozzi, C. R. A strain-promoted [3 + 2] azide–alkyne cycloaddition for covalent modification of biomolecules in living systems. *J. Am. Chem. Soc.* **126**, 15046–15047 (2004).
13. Agarwal, P., van der Weijden, J., Sletten, E. M., Rabuka, D. & Bertozzi, C. R. A Pictet-Spengler ligation for protein chemical modification. *Proc. Natl Acad. Sci. USA* **110**, 46–51 (2013).
14. Devaraj, N. K., Weissleder, R. & Hilderbrand, S. A. Tetrazine-based cycloadditions: application to pretargeted live cell imaging. *Bioconjugate Chem.* **19**, 2297–2299 (2008).
15. Lang, K. et al. Genetic encoding of bicyclononynes and trans-cyclooctenes for site-specific protein labeling in vitro and in live mammalian cells via rapid fluorogenic Diels–Alder reactions. *J. Am. Chem. Soc.* **134**, 10317–10320 (2012).
16. Fernández-Suárez, M. et al. Redirecting lipoic acid ligase for cell surface protein labeling with small-molecule probes. *Nat. Biotechnol.* **25**, 1483–1487 (2007).
17. Theile, C. S. et al. Site-specific N-terminal labeling of proteins using sortase-mediated reactions. *Nat. Protoc.* **8**, 1800–1807 (2013).
18. Meyer, C., Liebscher, S. & Bordusa, F. Selective coupling of click anchors to proteins via trypsiligase. *Bioconjugate Chem.* **27**, 47–53 (2016).
19. Kho, Y. et al. A tagging-via-substrate technology for detection and proteomics of farnesylated proteins. *Proc. Natl Acad. Sci. USA* **101**, 12479–1284 (2004).
20. Liebscher, S. et al. N-terminal protein modification by substrate-activated reverse proteolysis. *Angew. Chem. Int. Ed.* **53**, 3024–3028 (2014).
21. Arnison, P. G. et al. Ribosomally synthesized and post-translationally modified peptide natural products: overview and recommendations for a universal nomenclature. *Nat. Prod. Rep.* **30**, 108–160 (2013).
22. Montalbán-López, M. et al. New developments in RIPP discovery, enzymology and engineering. *Nat. Prod. Rep.* **38**, 130–239 (2021).
23. Morinaka, B. I. et al. Natural noncanonical protein splicing yields products with diverse β-amino acid residues. *Science* **359**, 779–782 (2018).
24. Lai, S., Mao, W., Song, H., Xia, L. & Xie, H. A biocompatible inverse electron demand Diels–Alder reaction of aldehyde and tetrazine promoted by proline. *New J. Chem.* **40**, 8194–8197 (2016).
25. Xie, H. et al. Proline-catalyzed direct inverse electron demand Diels–Alder reactions of ketones with 1,2,4,5-tetrazines. *Org. Lett.* **10**, 1923–1926 (2008).
26. Bohne, C., MacDonald, I. D. & Dunford, H. B. Transient state kinetics of the reactions of isobutyraldehyde with compounds I and II of horseradish peroxidase. *J. Biol. Chem.* **262**, 3572–3578 (1987).
27. Lakis, E., Magyari, S. & Piel, J. In-vivo production of diverse β-amino acid-containing proteins. *Angew. Chem. Int. Ed.* **61**, e202202695 (2022).
28. Ballantyne, A. & Dhillon, S. Trastuzumab emtansine: first global approval. *Drugs* **73**, 755–765 (2013).
29. Sehlin, D. et al. Antibody-based PET imaging of amyloid beta in mouse models of Alzheimer's disease. *Nat. Commun.* **7**, 10759 (2016).
30. Conner, K. P. et al. Evaluation of near infrared fluorescent labeling of monoclonal antibodies as a tool for tissue distribution. *Drug Metab. Dispos.* **42**, 1906–1913 (2014).
31. Kumar, A., Planchais, C., Fronzes, R., Mouquet, H. & Reyes, N. Binding mechanisms of therapeutic antibodies to human Cd20. *Science* **369**, 793–799 (2020).
32. Khongorzul, P., Ling, C. J., Khan, F. U., Ihsan, A. U. & Zhang, J. Antibody–drug conjugates: a comprehensive review. *Mol. Cancer Res.* **18**, 3–19 (2020).
33. Muyldermans, S. Nanobodies: natural single-domain antibodies. *Annu. Rev. Biochem.* **82**, 775–797 (2013).
34. Plückthun, A. Designed ankyrin repeat proteins (Darpins): binding proteins for research, diagnostics, and therapy. *Annu. Rev. Pharmacol. Toxicol.* **55**, 489–511 (2015).
35. Frejd, F. Y. & Kim, K.-T. Affibody molecules as engineered protein drugs. *Exp. Mol. Med.* **49**, e306–e306 (2017).
36. Orlova, A. et al. Tumor imaging using a picomolar affinity Her2 binding Affibody molecule. *Cancer Res.* **66**, 4339–4348 (2006).
37. Ahlgren, S. et al. Evaluation of maleimide derivative of DOTA for site-specific labeling of recombinant affibody molecules. *Bioconjugate Chem.* **19**, 235–243 (2008).
38. Alley, S. C. et al. Contribution of linker stability to the activities of anticancer immunoconjugates. *Bioconjugate Chem.* **19**, 759–765 (2008).
39. Baldwin, A. D. & Kiick, K. L. Tunable degradation of maleimide–thiol adducts in reducing environments. *Bioconjugate Chem.* **22**, 1946–1953 (2011).
40. Scott, T. A. et al. Widespread microbial utilization of ribosomal β-amino acid-containing peptides and proteins. *Chem.* **8**, 2659–2677 (2022).
41. Moore, D. A., Whatley, Z. N., Joshi, C. P., Osawa, M. & Erickson, H. P. Probing for binding regions of the FtsZ protein surface through site-directed insertions: discovery of fully functional FtsZ-fluorescent proteins. *J. Bacteriol. Res.* **199**, e00553-16 (2016).

42. Ma, X., Ehrhardt, D. W. & Margolin, W. Colocalization of cell division proteins FtsZ and FtsA to cytoskeletal structures in living *Escherichia coli* cells by using green fluorescent protein. *Proc. Natl Acad. Sci. USA* **93**, 12998–13003 (1996).
43. Gardner, K. A., Moore, D. A. & Erickson, H. P. The C-terminal linker of *Escherichia coli* FtsZ functions as an intrinsically disordered peptide. *Mol. Microbiol.* **89**, 264–275 (2013).
44. Yu, J., Liu, Y., Yin, H. & Chang, Z. Regrowth-delay body as a bacterial subcellular structure marking multidrug-tolerant persisters. *Cell Discov.* **5**, 8 (2019).
45. Kenworthy, A. K. Imaging protein–protein interactions using fluorescence resonance energy transfer microscopy. *Methods* **24**, 289–296 (2001).
46. Widder, P., Schuck, J., Summerer, D. & Drescher, M. Combining site-directed spin labeling in vivo and in-cell EPR distance determination. *Phys. Chem. Chem. Phys.* **22**, 4875–4879 (2020).
47. Jumper, J. et al. Highly Accurate protein structure prediction with AlphaFold. *Nature* **596**, 583–589 (2021).
48. Varadi, M. et al. AlphaFold protein structure database: massively expanding the structural coverage of protein-sequence space with high-accuracy models. *Nucleic Acids Res.* **50**, D439–D444 (2021).
49. Eigenbrot, C., Ultsch, M., Dubnovitsky, A., Abrahmsén, L. & Härd, T. Structural basis for high-affinity Her2 receptor binding by an engineered protein. *Proc. Natl Acad. Sci. USA* **107**, 15039–15044 (2010).

Methods

General

All reagents were purchased from commercial sources and used as received. Solvents were procured from Sigma-Aldrich and used as received. Double-distilled water was obtained from a PURELAB Chorus system (ELGA Veolia). Oligonucleotides for molecular cloning were synthesized by Microsynth (Switzerland). Plasmids were purified with the NucleoSpin plasmid purification kit purchased from Macherey-Nagel (Germany), agarose gel purifications were carried out with the NucleoSpin Gel and PCR Clean-up kit (Macherey-Nagel). Q5 Site-Directed Mutagenesis kit, restriction enzymes, T4 DNA ligase and Q5 DNA polymerases were purchased from New England Biolabs (NEB). Antibiotics (chloramphenicol, kanamycin and ampicillin) were purchased from Applichem. GluC endoprotease was purchased from NEB, and sequencing-grade trypsin endoprotease was purchased from Promega. Bacteria lysis was done on Qsonica Q700 sonicator equipped with either a 2 or 6 mm probe. Protino agarose Ni-NTA resin was purchased from Macherey-Nagel. Nuclear magnetic resonance (NMR) spectra were acquired on a Bruker 300 (AV III), Bruker 400 (Ascend, Ult) or Bruker 500 (Avn) instrument using TopSpin 3.5./4.1 (Bruker). ^{1}H-NMR chemical shifts are reported in p.p.m. relative to $SiMe_4$ ($\delta = 0$) and were referenced internally with respect to residual protons in the solvent ($\delta = 7.26$ for $CDCl_3$, $\delta = 2.50$ for dimethyl sulfoxide (DMSO)-d_6). Coupling constants are reported in Hz. ^{13}C-NMR chemical shifts are reported in p.p.m. relative to $SiMe_4$ ($\delta = 0$) and were referenced internally with respect to solvent signal ($\delta = 77.16$ for $CDCl_3$). Peak assignments are based on calculated chemical shift and multiplicity. Splitting patterns are reported as follows: singlet (s), doublet (d), triplet (t), quartet (q) and multiplet (m). LC–MS experiments were performed on a Dionex Ultimate 3000 UHPLC equipped with columns from Phenomenex and coupled to a mass spectrometer. Mass spectra were acquired on an LTQ Orbitrap XL or Q Exactive (Thermo Fisher Scientific) spectrometer by using heated electrospray ionization. Thin-layer chromatography was performed using commercial Merck silica gel plates, and components were visualized with UV ($\lambda = 254$ nm). Model structures were predicted using the online Colab version of AlphaFold[47,48,50]. IUPAC names of all compounds are provided and were determined using CS ChemDraw Professional 18.0. LC–MS data were analysed with the Thermo Xcalibur Qual browser 4.1 (Thermo Fisher Scientific). For vector graphic creation, the open-source software Inkscape 0.92 was used.

Plasmid construction

All plasmids used in this study are listed in Supplementary Table 2. Protein expression plasmids were constructed by Gibson Assembly Cloning (for genes >100 base pairs) or the Q5® site-directed mutagenesis (for genes <100 base pairs) protocol provided by NEB. Gene assembly fragments were designed by NEBuilder tool online. Overlapping mutagenic primers were designed by NEBaseChanger tool online. A typical polymerase chain reaction (PCR) (50 µl) contained 20 ng template DNA, 1× Q5 reaction buffer, 200 µM dNTPs, 0.5 µM of each primer (Supplementary Table 1) and 0.5 U Q5 High-Fidelity DNA Hot-Start Polymerase. The reaction was heated to 98 °C for 45 s followed by 35 cycles of 98 °C for 10 s, *X* °C for 20 s, and 72 °C for 20 s per kilobase DNA target sequence. The primer annealing temperature *X* was calculated with the NEB Tm calculator website or the NEBaseChanger (in case of the Q5 site-directed mutagenesis protocol). The resulting PCR amplicons were treated with kinase-ligase-DpnI mix (KLD mix, NEB). Gibson Assembly was performed with Gibson Assembly Master Mix (NEB) according to the manufacturer's instructions. DNA was visualized by 1% (w/v) agarose gel electrophoresis supplemented with ethidium bromide and GeneRuler 1 kb DNA ladder (Thermo Scientific) marker. Plasmids were transformed into chemically competent *E. coli* DH5α strain (Invitrogen) and grown on LB agar containing appropriate antibiotics, then inoculated in corresponding liquid LB medium. Plasmids were isolated from fresh overnight cultures, and the gene of interest was sequence-verified by Microsynth. All plasmids are under isopropyl-β-D-1-thiogalactopyranoside regulation. pACYCDuet encodes chloramphenicol resistance, pRSFDuet kanamycin resistance and pRM006 ampicillin resistance.

Small-molecule studies

For additive studies, model compound **1** (100 µM) was dissolved H_2O or PBS and added with 3,6-di-2-pyridyl-1,2,4,5-tetrazine **2** (100 µM), then supplied with additives L-proline (50 µM), $CaCl_2$ (1 mM) and/or $MgCl_2$ (1 mM). The samples were incubated overnight at 37 °C and analysed by LC–MS. Relative product formation of **4** and **5** was analysed by comparing area under the curve for the respective masses in the chromatogram, normalizing to the highest conversion rate. From the MS data, the area under the curve for $m/z = 531.2139$ (for **4**) or $m/z = 423.1564$ (for **5**) were extracted. Data analysis and statistical analysis were done in Microsoft Excel (2016) and Prism 9 (GraphPad).

Stability measurements

Stability of **4** and **5** in aqueous solutions was measured by dissolving purified **4** or **5** in 50% acetonitrile in H_2O to obtain 10 mM solutions. From these samples, 5 µl was then analysed every 24 h by LC–MS with method B over the course of 3 days, incubating at room temperature in between. Areas under the curve for UV traces (280 nm) were plotted against time. Measurements were done in triplicates.

Kinetic measurements

For kinetic measurements, 140 µl H_2O or PBS were added with 20 µl of a 10 mM stock solution of **1** in DMSO (final concentration 1 mM) and 20 µl, 40 µl or 80 µl of a 5 mM stock solution of **2** in DMSO (final concentrations: 0.5 mM, 1 mM or 2 mM) in a 96-well plate. Wells were filled up to 200 µl with DMSO (final mixture: H_2O/DMSO: 70/30). Alternatively 10 µl, 20 µl or 40 µl of a 10 mM stock solution of (4-(1,2,4,5-tetrazin-3-yl) phenyl)methanamine hydrochloride (compound **8**) in DMSO was added and filled up to 200 µl with DMSO. Absorbance at 515 nm was monitored over time every minute on a BioTek Synergy H1 plate reader (Agilent). Before every measurement, samples were shaken for 1 s. Measurements were done in triplicates. Control samples without **1**, **2** or **8** were prepared by using the appropriate amount of DMSO. For each sample the signal change of just **1** in H_2O was subtracted and the absorbance converted to a concentration of **2** or **8**. The reciprocal concentration of remaining tetrazine reagent versus time were plotted to yield a second-order rate constant through linear regression. Data analysis and statistical testes were done in Microsoft Excel (2016) and Prism 9 (GraphPad).

Enolization studies

To determine the amount of enol present and k_{obs} for the enolization of **1** in solution, a 10 mM stock solution of **1** in DMSO was diluted with either H_2O, D_2O or deuterated PBS 1:100 (100 µM final concentration). Samples were then directly injected on a Dionex Ultimate 3000 coupled to a Q Exactive mass spectrometer. Samples were then re-injected every 30 min to measure the change in signal of **1** versus deuterated **1** or doubly deuterated **1**. The remaining fraction of **1** was then plotted to yield a half life of **1** towards the enolization reaction and the corresponding rate constant. The fraction of **1** observed in the very first measurement was assumed to yield the initial amount of enol present in either D_2O or PBS due to the enol exchanging its proton faster than the keto form. Kinetic isotope effects were not considered in this study. Measurements were done in triplicates and statistical tests done in Prism 9 (GraphPad).

Affibody-splicease motif fusion cloning

Protein expression plasmid *his*$_6$-*z*$_{Her2:342}$-*gyg*/pACYCDuet-1 encoding His_6-$Z_{Her2:342}$-GYG was generated by Gibson assembly. The *z*$_{Her2:342}$-*gyg* gene was cloned into the multiple cloning site 1 of the pACYCDuet-1

vector in frame with the N-terminal His_6-tag. The assembly PCR was carried out with overlapping Her2:342_UP and Her2:342_DOWN synthetic oligonucleotides (Supplementary Table 1) and pACYCDuet-1 as template DNA. The plasmid *his_6-$z_{Her2:342}$-cys*/pACYCDuet-1 encoding His_6-$Z_{Her2:342}$-Cys was constructed by full plasmid amplification with *his_6-$z_{Her2:342}$-gyg*/pACYCDuet-1 as template and mutagenic primers (Supplementary Table 1).

FtsZ-splicease motif fusion cloning

The protein expression plasmid *ftsZ*/pRM006 encoding His_6-SUMO tagged FtsZ was purchased from Addgene (#98922). The *ftsZ*/pRM006 was used as a template DNA for subsequently generating plasmids for expressing FtsZ fusions with the splice tag at the N-terminus and between E35-G35, A53-V54 and G55-Q56. These constructs were made by full plasmid amplification with mutagenic primers named after the corresponding plasmid constructs (Supplementary Table 1).

The FtsZ gene was subcloned also into pACYCDuet-1 vector, multiple cloning site 1 in frame with N-teminal His_6-tag by Gibson assembly. The linear FtsZ gene was PCR amplified from *ftsZ*/pRM006 as the template with overlapping primers FtsZ gene_fwd, FtsZ gene_rev. The pACYCDuet-1 vector was used as a template for full plasmid amplification by PCR using pACYCDuet1_fwd and pACYCDuet1_rev primers. Primers were designed in NEBuilder tool online. Assembly of PCR products yielded *ftsZ*/pACYCDuet-1 plasmid, which was used as a template DNA for splice tag insertion by Q5 site-directed mutagenesis. The splicing motif was inserted between L325-D337, E350-Q364 and at N- and C-terminus of FtsZ. The same name was given to primers and plasmids as for the corresponding insertion site (Supplementary Table 1).

Protein expression and purification

A Falcon tube containing 5 ml of LB medium was inoculated with *E. coli* BL21 (DE3) cells taken from previously prepared glycerol stocks or from single colonies on agar plates and supplemented with the appropriate antibiotics. The culture was shaken at 180 to 220 r.p.m. overnight at 37 °C.

On the next day, 30–800 ml TB medium containing the appropriate antibiotics was inoculated with 1% v/v of this overnight culture and shaken at 37 °C until an OD_{600} of 1.4–1.8 was reached, according to previously reported expressions in similar systems[23]. After cooling the cultures at 4 °C for at least 20 min, 1 mM of isopropyl-β-D-1-thiogalactopyranoside was added and the cultures were incubated on a shaker at 180–220 r.p.m. at 16–24 °C for approximately 16–20 h. Subsequently, the cultures were centrifuged at 6,000*g* for 10 min at 4 °C. The supernatant was discarded, and the cell pellets resuspended in 1–25 ml NPI-10 buffer. All NPI buffers were supplemented with 10% glycerol.

All volumes were adjusted to scale with the culture volume (for example, 1 ml NPI-10 buffer for resuspension was used for 30 ml cultures, and 10 ml NPI-10 buffer were used for resuspension of cells grown in 300 ml medium). NPI buffers contain 50 mM NaH_2PO_4, 300 mM NaCl and 10–250 mM imidazole and are adjusted to pH 8.0.

Cells resuspended in NPI-10 buffer were sonicated for 10 times 10 s, with 10 s of pause in between, at an amplitude of 25–40. A sonication tip with a radius of 2–6 mm was used, depending on the volume to be sonicated. The resulting suspensions were kept on ice and centrifuged at 21,000*g* for 30 min at 4 °C.

The supernatant was transferred to a new tube and 125 µl to 2 ml of Protino Ni-NTA Agarose (Macherey-Nagel) was added. The samples were slowly shaken on a rotor at 10 r.p.m. for at least 30 min. An appropriate column was pre-washed with NPI-10 buffer, the sample added, washed twice with NPI-10 (500 µl to 10 ml), twice with NPI-20 (500 µl to 10 ml) and the protein eluted with NPI-250 (550 µl to 10 ml) and collected. Elution fractions were digested with appropriate endoproteinases. Protein splicing was analysed by high-resolution LC–MS. Samples were stored at −20 °C for further use.

General protein labelling reactions

Ni-NTA affinity-purified proteins containing aminopyruvate residues were generally incubated in NPI-250 buffer with 100 µM (**2** and **7**) or 1–10 µM (**6**) for 18 h at 37 °C. Reactions were then directly analysed by LC–MS for full proteins or first digested with appropriate endoproteases.

Proteins labelled with a tetrazine probe conjugated to a fluorescent dye (CF®488A tetrazine **6**, Chemie Brunschwig AG) were run on sodium dodecyl sulfate polyacrylamide gel electrophoresis (SDS–PAGE) after incubation overnight at 37 °C. The gels were analysed by a fluorescent imager with a band pass filter 532/28 (ChemiDoc MP, Bio-Rad), followed by staining with Coomassie Brilliant Blue and subsequent destaining (10% AcOH, 30% MeOH and 60% H_2O) overnight.

$Z_{Her2:342}$-TyrEx-DOTA and $Z_{Her2:342}$-Cys-DOTA conjugation and purification

The $Z_{Her2:342}$-TyrEx-DOTA conjugation reaction was prepared by adding DOTA-tetrazine **7** (10 µl, 1 mM solution in DMSO) to the splice-tagged protein solutions in NPI-250 buffer. Following incubation overnight at 37 °C, reaction mixtures were loaded to solid phase extraction columns (Strata-X 100 mg/3 ml, Phenomenex) pre-equilibrated first with 10 column volumes acetonitrile and subsequently with 10 column volumes H_2O. Columns were washed with 10 column volumes 5% acetonitrile/H_2O + 0.1% formic acid. Protein conjugates were eluted with 10 column volumes 30% acetonitrile/H_2O + 0.1% formic acid. Resulting elutions were purified by reversed-phase HPLC on a Phenomenex Luna 5 µm Phenyl-Hexyl column (250 × 4.6 mm) with solvent A: H_2O + 0.1% trifluoroacetic acid, solvent B: acetonitrile + 0.1% trifluoroacetic acid by the following gradient method: B 5% ramped up to 25% over the first 2 min, then a slow gradient to 29% at 14 min, then to 100% B over 1 min, 100% B for 2 min, then again 5% B for three more minutes to equilibrate. Fractions were analysed by LC–MS for purity and pure fractions combined.

$Z_{Her2:342}$-Cys-DOTA[37] was prepared from Ni-NTA elutions (2 mg ml^{-1}) by first reducing the protein solutions with 30 µM dithiothreitol for 2 h at 37 °C and removal of excess dithiothreitol by PD-10 desalting columns pre-equilibrated with 20 mM ascorbic acid. Then 900 µl of the resulting elution was mixed with DOTA maleimide (200 µl, 1 mg ml^{-1}) and NH_4OAc (300 µl, 1 M, pH 5.5). The reaction mixtures were incubated overnight at 37 °C, desalted by PD-10 desalting columns pre-equilibrated with 200 mM NH_4OAc, then purified by reversed-phase HPLC with the same conditions as $Z_{Her2:342}$-TyrEx-DOTA.

Purified proteins were dried on a small-scale rotary evaporator (Eppendorf Concentrator 5301) and resuspended in PBS. Protein concentrations were measured by ROTI Nanoquant assay (Carl Roth).

ELISA

$Z_{Her2:342}$-TyrEx-DOTA (5 µM), $Z_{Her2:342}$-GYG (1.875 µM), $Z_{Her2:342}$-Cys (5 µM), $Z_{Her2:342}$-TyrEx-Cys-DOTA (10 µM) and Her2 commercial Affibody (5 µM) were prepared as solutions in PBS at the given concentrations. The assay was carried out with a Her2-coated plate and buffers from an *EDI*™ Humanized Anti-Her2/neu (Herceptin/trastuzumab) ELISA Kit (Epitope Diganostics) following the manufacturer's protocol. A 4× dilution series of each sample in 200 µl was prepared in duplicates in a 96-well transfer plate with the supplied assay buffer. Samples (100 µl) were then transferred to the Her2-coated plate and incubated at 22 °C on an orbital shaker at 400 r.p.m. for 90 min. Each well was washed five times with the supplied wash buffer, and 100 µl Goat Anti-Affibody IgG (Affibody SE) 0.5 µg ml^{-1} in assay buffer was added to each well, then incubated at 22 °C at 400 r.p.m. for 60 min. Each well was washed five times with the supplied wash buffer and 100 µl anti-goat IgG (Fc specific)-peroxidase antibody (Sigma-Aldrich), 50 ng ml^{-1} in assay buffer was added to each well, and the plate was then incubated at 22 °C at 400 r.p.m. for 60 min. Each well was washed five times with wash buffer, 100 µl of the supplied horseradish peroxidase substrate

solution was added to each well, and the plate was wrapped with aluminium foil and incubated at room temperature in the dark for 30 min. The reaction was stopped by the addition of 100 µl of the supplied stop solution. Absorption at 450 nm was measured with a Victor3 (PerkinElmer) spectrophotometer. Binding curves and sigmoidal fits were constructed in GraphPad Prism 9.

Blood plasma stability

$Z_{Her2:342}$-TyrEx-DOTA, $Z_{Her2:342}$-GYG, and $Z_{Her2:342}$-Cys-DOTA (135 µg ml^{-1}, 25 µl) and 25 µl human blood plasma (Sigma-Aldrich) were mixed and incubated at 37 °C in triplicates. After 0, 1, 4, 8, 24 and 72 h, 10 µl was removed from the solutions and stored at −80 °C until LC–MS analysis. Samples were mixed with 25 µl of 75% acetonitrile in water to precipitate blood plasma proteins. Samples were subjected to LC–MS after centrifugation (2 × 20,000*g* for 10 min). Intensities of deconvoluted mass ions for $Z_{Her2:342}$-TyrEx-DOTA, $Z_{Her2:342}$-GYG and $Z_{Her2:342}$-Cys-DOTA respective conjugates were recorded. Intensities were normalized to the $t = 1$ h timepoint and plotted against incubation time.

Labelling proteins with a fluorescent tetrazine in *E. coli* cells

E. coli BL21 (DE3) cells harbouring precursor and splicease plasmids were grown according to the protein expression procedure. Cells were taken from the culture and diluted to an OD_{600} of 0.4–0.6 with PBS (pH 7.4, final volume: 3 ml). The samples were centrifuged (7,000*g*, 5 min), the supernatant discarded and the cells resuspended in PBS (3 ml). Samples were again centrifuged and resupended in PBS containing 0.3% Triton X-100 and 100 µM CF®488A tetrazine **6**. Samples were incubated for 60 min at 16 °C, then then centrifuged (7,000*g*, 5 min), the supernatant discarded and the cells resuspended in PBS (1 ml). This wash was repeated once. Samples were then lysed by sonication and purified according to the general Ni-NTA affinity purification protocol. Elution fractions were concentrated on Vivaspin 500 concentrators (molecular weight cut-off 3 kDa) and were run on SDS–PAGE. The gels were analysed by a fluorescent imager with a band pass filter 532/528 (ChemiDoc MP, Bio-Rad), followed by staining with Coomassie Brilliant Blue and subsequent destaining (10% AcOH, 30% MeOH and 60% H_2O) overnight.

Labelling proteins with a fluorescent tetrazine in *E. coli* cells and preparation for microscopy

E. coli BL21 (DE3) cells harbouring precursor and splicease plasmids were grown according to the protein expression procedure. Cells were taken from the culture and diluted to an OD_{600} of 0.4–0.6 with PBS (pH 7.4, final volume: 100 µl). The samples were centrifuged (7,000*g*, 5 min), the supernatant discarded and the cells resuspended in PBS (100 µl). Samples were incubated with 4% formaldehyde for 30 min, then washed twice with PBS. Samples were incubated with 0.3% Triton X-100 at room temperature for 30 min, then washed twice with PBS. Samples were incubated with 100 µM CF®488A tetrazine for 60 min at 16 °C, then centrifuged (7,000*g*, 5 min), the supernatant discarded and the cells resuspended in PBS (100 µl). This wash was repeated twice. Samples (1–3 µl) were then added to a cover slip and covered with 1.5% w/v agarose pad for imaging. From these samples, regions of interest were located using the brightfield mode on the microscope, and *z*-stacks were recorded in brightfield and at 488 nm (200 mW, 30% power, 400 ms).

Samples were imaged on an Axiovert 200 m (inverse) microscope, equipped with a Yokogawa CSU-X1 spinning-disk confocal unit and a LUDL BioPrecision2 stage with Piezo Focus. Images were acquired with an sCMOS camera (Orca Flash 4.0 V). Diode-pumped solid-state lasers were used as light sources, where the 488 nm (200 mW) laser was used. A 100× 1.4 CFI Plan Apo Oil objective was used for all image acquisitions. Emitted light was filtered using the GFP (ET 525/550) filter. The microscope was operated using the VisiVIEW (Metamorph) software. Image analysis was performed with Fiji (ImageJ).

High-resolution MS

Mass spectra were acquired on an LTQ Orbitrap XL or Q Exactive (Thermo Fisher Scientific) spectrometer by using heated electrospray ionization. The following method was used for analysis on LC–MS:

Solvent A, H_2O + 0.1% formic acid; solvent B, MeCN + 0.1% formic acid; column, Phenomenex Kinetex 2.6 µm C18-XB 100 Å (150 × 4.6 mm); flow rate, 1.0 ml min^{-1}; gradient: 95:5 A/B for 0.5 min ramped to 5:95 A/B over 20 min).

For MS/MS analysis a normalized collision energy of 15–28 was used, depending on the observed fragmentation properties of peptide fragments. The MS was operated in positive ionization mode at a scan range of 150–2,000 *m*/*z*, automatic gain control target 2×10^5, maximum injection time 100 ms and a resolution of 70,000 at 400 *m*/*z*. The spray voltage was set to 5.0 kV, probe heater temperature to 475 °C and capillary temperature to 270 °C. Columns were heated to 50 °C for methods A and C.

Reporting summary

Further information on research design is available in the Nature Portfolio Reporting Summary linked to this article.

Data availability

The data supporting the findings of this study are available in this article and Supplementary Information. The crystal structure of the affibody $Z_{Her2:342}$ was downloaded from the RCSB PDB (PDB 3MZW). Source data are provided with this paper.

Reference

50. AlphaFold Colab. *Colab* https://colab.research.google.com/github/deepmind/alphafold/blob/main/notebooks/AlphaFold.ipynb (2022).

Acknowledgements

The authors are grateful for funding from the European Research Council (ERC; ERC Advanced Project SynPlex, 742739) and the ETH (Research Grant ETH-21 21-2). We thank D. Neri and F. Frejd for insightful discussions.

Author contributions

D.R., E.L. and J.P. designed the research and experiments. D.R. performed synthetic steps, aminopyruvate model studies, His_6-PlpA3-M5G experiments and $Z_{Her2:342}$ affibody purification and assays. E.L. conducted FtsZ tag location studies and microscopy experiments. All authors contributed to manuscript writing.

Funding

Open access funding provided by Swiss Federal Institute of Technology Zurich.

Competing interests

D.R., E.L. and J.P. are inventors on patent application EP21200343.8 submitted by ETH Zurich that covers the method for preparation of pyridazine compounds from aminopyruvate and tetrazines.

Additional information

Supplementary information The online version contains supplementary material available at https://doi.org/10.1038/s41557-023-01252-8.

Correspondence and requests for materials should be addressed to Jörn Piel.

Peer review information *Nature Chemistry* thanks the anonymous reviewers for their contribution to the peer review of this work.

nature research

Corresponding author(s): Professor Jörn Piel

Last updated by author(s): Apr 25, 2023

Reporting Summary

Nature Research wishes to improve the reproducibility of the work that we publish. This form provides structure for consistency and transparency in reporting. For further information on Nature Research policies, see our Editorial Policies and the Editorial Policy Checklist.

Statistics

For all statistical analyses, confirm that the following items are present in the figure legend, table legend, main text, or Methods section.

n/a	Confirmed	
☐	☒	The exact sample size (*n*) for each experimental group/condition, given as a discrete number and unit of measurement
☐	☒	A statement on whether measurements were taken from distinct samples or whether the same sample was measured repeatedly
☐	☒	The statistical test(s) used AND whether they are one- or two-sided *Only common tests should be described solely by name; describe more complex techniques in the Methods section.*
☒	☐	A description of all covariates tested
☒	☐	A description of any assumptions or corrections, such as tests of normality and adjustment for multiple comparisons
☐	☒	A full description of the statistical parameters including central tendency (e.g. means) or other basic estimates (e.g. regression coefficient) AND variation (e.g. standard deviation) or associated estimates of uncertainty (e.g. confidence intervals)
☐	☒	For null hypothesis testing, the test statistic (e.g. *F*, *t*, *r*) with confidence intervals, effect sizes, degrees of freedom and *P* value noted *Give P values as exact values whenever suitable.*
☒	☐	For Bayesian analysis, information on the choice of priors and Markov chain Monte Carlo settings
☒	☐	For hierarchical and complex designs, identification of the appropriate level for tests and full reporting of outcomes
☒	☐	Estimates of effect sizes (e.g. Cohen's *d*, Pearson's *r*), indicating how they were calculated

Our web collection on statistics for biologists contains articles on many of the points above.

Software and code

Policy information about availability of computer code

Data collection	MS acquisition: Xcalibur 4.1, Chromeleon Xpress 7.2 (Thermo Scientific); NMR acquisition: TopSpin 3.5./4.1 (Bruker); Microscopy: Visiview (Visitron)
Data analysis	MS: Xcalibur 4.1 (Thermo Scientific); NMR: MNova 14 (Mestrelab Research); Assays: Microsoft Excel 2019 (Microsoft), Prism 9.2 (GraphPad Software), Inkscape 0.92 (Open-source); DNA and protein sequences: Geneious 7.1.9 (Biomatters Limited.); Microscopy: Fiji 1.51 (Open-source)

For manuscripts utilizing custom algorithms or software that are central to the research but not yet described in published literature, software must be made available to editors and reviewers. We strongly encourage code deposition in a community repository (e.g. GitHub). See the Nature Research guidelines for submitting code & software for further information.

Data

Policy information about availability of data

All manuscripts must include a data availability statement. This statement should provide the following information, where applicable:

- Accession codes, unique identifiers, or web links for publicly available datasets
- A list of figures that have associated raw data
- A description of any restrictions on data availability

The data supporting the findings of this study are available in this article and the Supplementary Information. The crystal structure of the affibody was fetched from the RCSB PDB (PDB 3MZW).

Field-specific reporting

Please select the one below that is the best fit for your research. If you are not sure, read the appropriate sections before making your selection.

☒ Life sciences ☐ Behavioural & social sciences ☐ Ecological, evolutionary & environmental sciences

For a reference copy of the document with all sections, see nature.com/documents/nr-reporting-summary-flat.pdf

Life sciences study design

All studies must disclose on these points even when the disclosure is negative.

Sample size	Biological test were performed in triplicates ; sample size was chosen based on limited amounts of compounds.
Data exclusions	In the conditions experiment for (Figure 1) two values were excluded as the MS machine reported an error and did not measure properly
Replication	Labling with the reaction was performed on multiple substrates, in multiple attempts to verify reproducibility. Small molecule studies were all repeated 3 times with high reproduciblity. ELISA measurements were done in duplicates. Stability measurements of the Affibody constructs were done in triplicates with high reproduciblity. Representative microscopy images were taken from 3-12 images acquired for each condition
Randomization	Randomization was not relevant for this study, as we did not perform group comparisons.
Blinding	No blinding was performed in our study, as no group comparisons were performed and there was no specific reason to expect bias, as MS/MS and NMR are unbiased techniques.

Reporting for specific materials, systems and methods

We require information from authors about some types of materials, experimental systems and methods used in many studies. Here, indicate whether each material, system or method listed is relevant to your study. If you are not sure if a list item applies to your research, read the appropriate section before selecting a response.

Materials & experimental systems

n/a	Involved in the study
☐	☒ Antibodies
☒	☐ Eukaryotic cell lines
☒	☐ Palaeontology and archaeology
☒	☐ Animals and other organisms
☒	☐ Human research participants
☒	☐ Clinical data
☒	☐ Dual use research of concern

Methods

n/a	Involved in the study
☒	☐ ChIP-seq
☒	☐ Flow cytometry
☒	☐ MRI-based neuroimaging

Antibodies

Antibodies used	Only commercially available antibodies were used in ELISA for affibodies: Goat Anti-Affibody IgG (Affibody SE, catalog Nr. 20.1000.01.0005, Batch 1304-PB011), Anti-goat IgG (Fc specific)-Peroxidase antibody (Sigma Aldrich, catalog number SAB3700259-2MG, Lot RI34052)
Validation	Validation statments of the antibodies were supplied with the commercially available antibodies. Anti-goat IgG (Fc specific)-Peroxidase antibody was tested by ELISA, Western Blotting and Immunohistochemistry.